RESEARCH ARTICLE

Infrared Nonlinear Optical Performances of $(Ga_2Ge)_{100-x}(Ga_3Sb_2)_x$ (x = 15, 30, 45, 60) Thin Films

Rajnish Raj[1], Pooja Lohia[1], D. K. Dwivedi[2,]*

The traditional melt-quench technique was used to synthesize non-oxide $(Ga_2Ge)_{100-x}(Ga_3Sb_2)_x$ (x = 15, 30, 45, 60) glass alloys. The vacuum thermal evaporation unit was used to obtain thin films of prepared sample for investigation of optical properties. SEM, XRD and DSC technique were used to find the thermal and structural properties of the materials. The linear properties like optical bandgap, extinction coefficient for prepared samples have been studied in present paper of Ge-Ga-Sb for application of optoelectronics. The impurities present in the prepared thin films were defined by FTIR transmittance spectra. The extinction coefficient (k) value decreases with increase in Sb concentration while absorption coefficient (α). It was noticed that value of energy bandgap (E_g) derived from Tauc's plot varies from 2.9 eV to 1.25 eV. Urbach energy is inversely proportional to the bandgap of the materials. As the Sb concentration increases the band gap goes on decreases which result the increase in Urbach energy. Mott and Davis model has been used for explaining decrease in energy gap of prepared glassy alloys.

Introduction

The non-oxide glasses are appealing materials for various applications like distribution of thermal images, all such optical Raman amplification, infrared power, optical switching limiting, etc. [**1-5**]. The function of each kind of mechanism depends on various functions such as the sample preparation process, excitation wavelengths and so on [**6**]. The non-oxide glasses based on Ge-Sb-Ga-Se have high transition temperature that makes them a suitable host material for developing IR fiber amplifiers and lasers having high heat resistance, low optical losses and laser threshold damage.

Many researches have been carried out on non-oxide glasses for different optoelectronic applications. R. Tintu *et. al.*, studied the $Ga_5Sb_{10}Ge_{25}Se_{60}$ glasses and found that cluster size was responsible in tuning of optical bandgap of material [**7,8**]. E. V. Karaksina *et. al.*, studied the Ge-rich Ga-Ge-Sb-Se glass for thermal and optical studies and found that these glasses possess large glass transition temperature and tendency towards crystallization was very low. They also studied the refractive index of the prepared glassy alloys [**9,10**]. L. Petit *et. al.*, studied Ge-Sb-S non-oxide glasses and they found that addition of Sb increases linear refractive index, density as well as shift of absorption edge to infrared [**11**]. Therefore Ge-Sb-S are of interesting glasses for remarkable application as antioxidants over cladding layers of micro-resonator-based sensing [**12-15**].

Several other glasses compositions such as $Ge_{11.5}As_{24}Se_{64.5}$, $Ge_{10}As_{35}Se_{55}$ and Ge-As-Se have also significant properties such as high photo stability and nonlinearity [**16**]. However, Arsenic is toxic and environmentally un-recognized when devices based on Arsenic are disregarded, Antimony is an acceptable element. It has been found that the Sb transmission line can strengthen the optical nonlinearity of the glasses due to the more ionic existence of Sb [**17**].

In present paper we have introduced a new semiconducting non-oxide glasses $(Ga_2Ge)_{100-x}$ $(Ga_3Sb_2)_x$ (x = 15, 30, 45, 60). In this study, we have designed Ga and Sb-doped $(GeGa_2)_{100-x}(Sb_2Ga_3)_x$ (x = 15, 30, 45, 60) glass alloys system to discover glass both with lower T_g and higher T_c, that is important for passive and active both optical fibre drawing. The compositional dependence of parameters such as T_g, T_c, and the optical band gap was investigated. The optical and thermal effects of Sb addition to the $(Ga_2Ge)_{100-x}(Ga_3Sb_2)_x$ (x = 15, 30, 45, 60) have been comprehensively analyzed by means of DSC, UV-Vis and optical spectra of FTIR.

[1]Department of Electronics and Communication Engineering, M. M. M. University of Technology, Gorakhpur 273010, India
[2]Amorphous Semiconductor Research Lab, Department of Physics and Material Science, M. M. M. University of Technology, Gorakhpur 273010, India

*Corresponding author:
E-mail: todkdwivedi@gmail.com

DOI: 10.5185/amlett.2021.091662

Experimental

The semiconducting non-oxide glasses were prepared using well-known melt-quench technique using 5N pure Ge, Ga, and Sb elements purchased through Sigma-Aldrich. All pure elements were taken in quartz-ampoule in accordance with the true weight as calculated theoretically for compound and then sealed under high vacuum of 1×10^{-5} millibar. After sealing the ampoules were put in the melting furnace by attaching in ceramic rod with tungsten wire. The mixture was rotated while melting at some interval to maintain homogeneity of the samples. The temperature of muffle furnace was increased upto 850°C in steps of 5°C. The entire melting process of samples has taken 12 h for completing and after that the samples were quenched in ice-cooled water instantly for formation of bulk samples.

The thin films of the bulk samples were obtained using thermal evaporation method. The thermal evaporation process consists of evaporating and condensing processes in a vacuum ($\approx1\times10^{-5}$ millibar) chamber. The materials are evaporated by the heated source, which is at a few cm distances from a substrate. The evaporated particles are condensed on the substrate. Thickness of the thin film was measured by quartz crystal thickness monitor attached in vacuum coating unit [**18**]. The simple glass substrate was used for the deposition of thin films of prepared bulk glasses.

All the thin films have thickness 500 nm and were deposited on glass substrate at the 10-100 nm/min rate of deposition controlled at 5 MHz using a quartz crystal monitor. The X-ray diffraction of the prepared thin films were analyzed through X'Pert Pro in the 2θ range 10° to 80°. The step size was 0.02^0 while scan rate was 2^0/min. Grazing angle during experiment was 1^0. Surface morphology of the prepared sample was done by Zeiss EVO MA 15 Scanning Electron Microscope. SEM micrographs were obtained at accelerating voltages of 10 kV, 4.1 to 4.5 mm scanning area, 20 Pa chamber pressure and probe current varies between 200 pA (low mag) to about 50 pA (higher mag).

Thermal parameters of the samples were taken using differential scanning calorimetry (model: SHIMADZU DSC-60 Plus). The absorbance and transmittance of thin films were taken using ultraviolet-visible-near-infrared (UV-VIS) spectrophotometer (model: SHIMADZU UV-2600) in the range of 400-1000nm. IR transmittance spectra in the range of 400-5400 cm^{-1} was analyzed using FTIR spectroscopy (model: Perkin Elmer Spectrum Two). All the experiments were performed at room condition.

Results and discussion

Structural properties

The measurement of the X-ray diffraction of as prepared $(Ga_2Ge)_{100-x}$ $(Ga_3Sb_2)_x$ (x = 15, 30, 45, 60) material was recorded at an angle 2θ between 10^0 and 80^0 values. Absence of peaks in the pattern of XRD as shown in **Fig. 1** defines the amorphous nature of the material. SEM (Scanning Electron Microscopy) is a tool which gives the data of surface morphology of the prepared alloys. **Fig. 2** gives the surface morphology of the prepared thin films and from figure it is clear that the materials deposited on the glass substrates are homogeneous in nature.

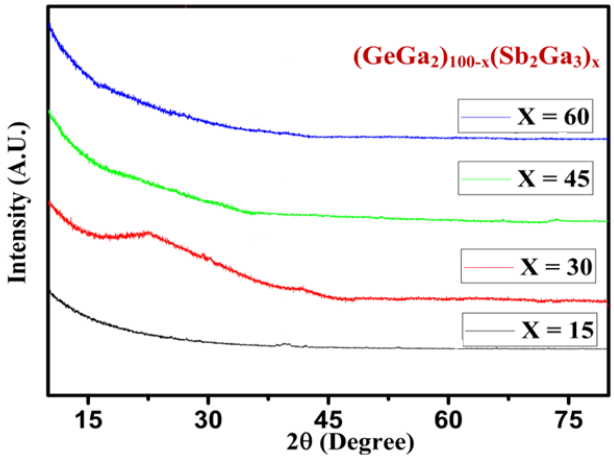

Fig 1. X-Ray Diffractogram pattern of $(Ga_2Ge)_{100-x}$ $(Ga_3Sb_2)_x$ (x = 15, 30, 45, 60) glasses.

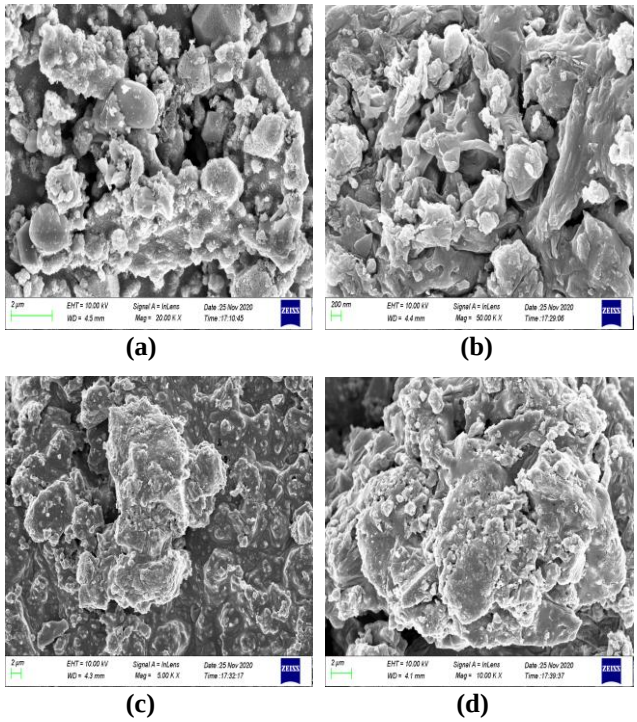

Fig 2. Scanning Electron Microscope of $(Ga_2Ge)_{100-x}(Ga_3Sb_2)_x$ (a) x=15, (b) x=30, (c) x=45, (d) x=60.

Thermal property

A Differential Scanning Calorimetry (DSC) is a strong method for estimating the sample's heat flow to change the temperature. The DSC measurement provide an

understanding of various thermo-dynamic transitions that allows us to determine the T_g (Glass Transition Temperature), T_c (Crystalline Temperature) and T_m (Melting point Temperature) of the $(Ga_2Ge)_{100-x}(Ga_3Sb_2)_x$ (x = 15, 30, 45, 60) sample. A DSC thermogram of all the selected samples is shown in **Fig 3**. From **Fig. 3** it was noticeable that there are two distinct characteristic points of the DSC thermogram, namely glass transition temperature (T_g) and crystallization temperature (T_c). All values of T_c and T_g are listed in the **Table 1** at a heating rate of 20 K/min. T_g is observed as increasing with doping concentration of x from 15 to 60. It can therefore be observed that in the prepared sample, Sb performs a dual behavior.

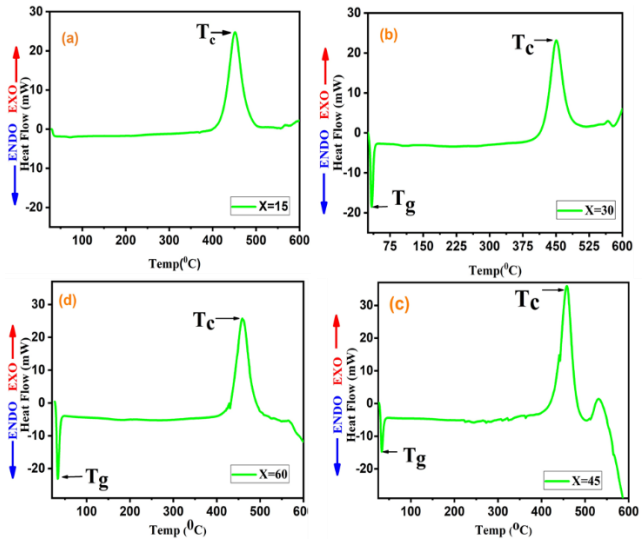

Fig 3. DSC thermo-graph of $(Ga_2Ge)_{100-x}(Ga_3Sb_2)_x$ at 20 K/min heating rate (a) x = 15 (b) x = 30 (c) x = 45 (d) x = 60 non-oxide alloy.

Table 1. T_g and T_c of $(GeGa_2)_{100-x}(Sb_2Ga_3)_x$(x = 15, 30, 45, 60) glassy alloy.

Composition $(GeGa_2)_{100-x}(Sb_2Ga_3)_x$	Glass Transition Temperature T_g (^{0}C)	Crystalline Temperature T_c (^{0}C)
x = 15	32.54	450.80
x = 30	33.65	451.20
x = 45	34.91	458.54
x = 60	35.34	460.56

Table 2. The possible values calculation of bond energy of $(GeGa_2)_{100-x}(Sb_2Ga_3)_x$ (x = 15, 30, 45, 60) thin films.

Bonds	Bond Energy (K cal / mol)
Ge – Sb	33.75
Ge – Ge	37.60
Ga – Ga	25.33
Ga - Ge	40.17
Ga – Sb	43.07
Sb - Sb	30.20

The variation in glass transition temperature could be attributed to the bond energy difference shown in **Table 2**. To evaluate the thermal stability of these glasses, multiple parameters are used. The two most popular parameters are differences between the value T_g and T_c, and the second criterion is Hruby parameter, which gives the ability to form glass [**19**]. The greater difference between the computed value of T_c and T_g suggests that the crystallization kinetic resistance is higher or vice versa. The glasses exhibiting the crystallization peak near the temperature of the glass transition are considered as unstable glasses, whereas glasses with a peak near the temperature of melting are considered stable glasses. Since the greater difference between T_c and T_g is for x = 60, suggesting the limit of the K parameter $(Ga_2Ge)_{40}(Sb_2Ga_3)_{60}$ has optimum thermal stability and, therefore, the ability to form large glass.

Optical properties

Infrared optical transmission spectra

Fig. 4 shows the IR optical transmission spectra of $(Ga_2Ge)_{100-x}$ $(Ga_3Sb_2)_x$ (x = 15, 30, 45, 60) glass alloys. Transmittance increases with wavenumber in the parent compound as shown in **Fig. 4**. The absorption band present in the transmittance spectra of the prepared sample is due to extrinsic impurities present in the sample because of preparation technique. The region from 3600 cm^{-1} – 5400 cm^{-1} contains no absorption band; hence this region can be used for different IR applications [**20-22**]. The absorption band present in the range 2230–3580 cm^{-1} refers to the impurities caused by Ge-O, Ga-O bonds. The absorption band at 3580 cm^{-1} refers to the impurity exist because of absorbed water molecules.

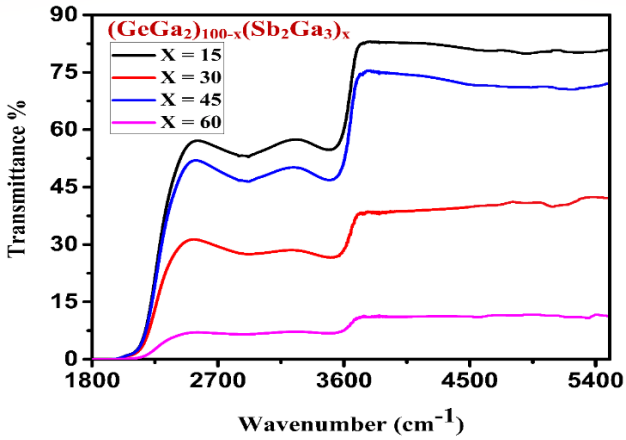

Fig 4. IR transmittance spectra of $(Ga_2Ge)_{100-x}(Ga_3Sb_2)_x$ (x = 15, 30, 45, 60) glassy thin films.

Optical band gap and absorption coefficient analysis

The transmittance spectra obtained by UV-Vis spectrophotometer for all $(Ga_2Ge)_{100-x}$ $(Ga_3Sb_2)_x$ (x = 15, 30, 45, 60) thin film samples was used for calculating different optical constants like extinction coefficient (k), absorption coefficient (α) and optical band gap (E_g). **Fig. 5** shows the Transmittance spectra of prepared glassy semiconductors. The increase in the transmittance spectra was observed with the increase in wavelength. The maximum transmittance at 900 nm wavelength was found

for all $(Ga_2Ge)_{100-x}$ $(Ga_3Sb_2)_x$ (x = 15, 30, 45, 60) thin film samples. Moreover, it is also found that for Sb doping (x = 45) of $(Ga_2Ge)_{100-x}$ $(Ga_3Sb_2)_x$ compound has higher transmittance among Sb (x = 15, 30, 60) doping.

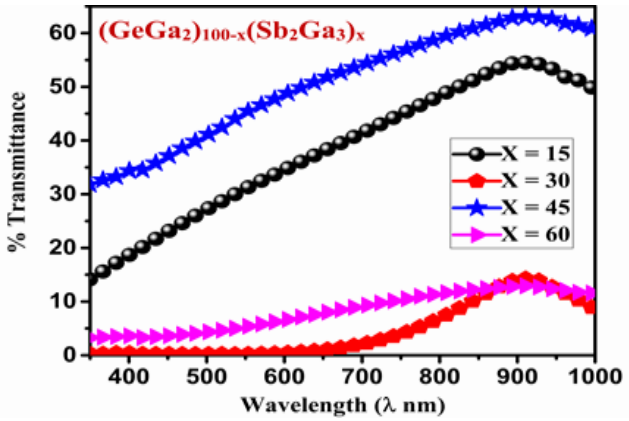

Fig 5. The spectral variation of the %Transmission for prepared thin films $(Ga_2Ge)_{100-x}(Ga_3Sb_2)_x$ for (x = 15, 30, 45, 60).

The absorption coefficient (α) [**23-25**] is obtained by using absorbance (A) of the thin films by following formula:

$$\text{Absorption coefficient } (\alpha) = \frac{2.303\ A}{t} \quad (1)$$

where,

$$\text{Absorbance} = 2 - \log(\%\text{Transmittance}) \quad (2)$$

The thickness (t) of the samples were recorded using quartz crystal monitor attached in setup of vacuum thermal coating unit. The variation of absorption coefficient (α) with photon energy (hν) of $(Ga_2Ge)_{100-x}$ $(Ga_3Sb_2)_x$ (x = 15, 30, 45, 60) thin films is shown in **Fig. 6**. It was observed that value of α shows increasing behavior with photon energy and it was also observed that increasing Sb constituent increases the absorption coefficient of the samples. The increase in absorption coefficient with Sb addition may be due to increased photosensitivity of the material and greater absorption of light by the thin films.

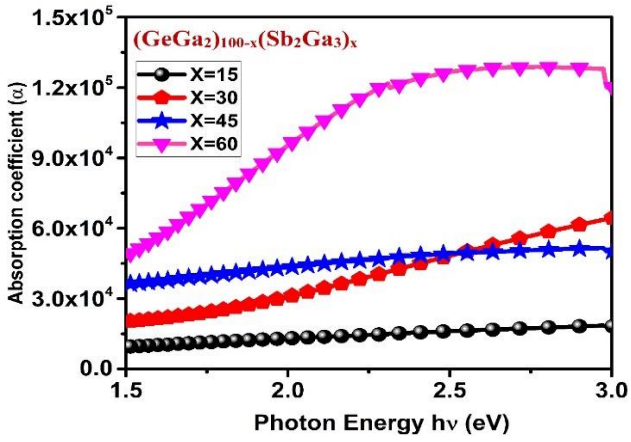

Fig 6. The distribution of "α" varies photon energy "hν"(eV) of $(Ga_2Ge)_{100-x}(Ga_3Sb_2)_x$ (x = 15,30, 45, 60).

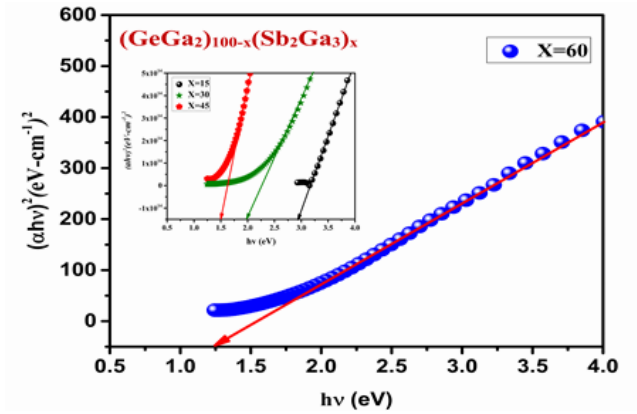

Fig 7. Variation between photon energy (hν) vs $(\alpha h\nu)^{1/n}$ of $(GeGa_2)_{100-x}(Sb_2Ga_3)_x$ (x = 15,30, 45, 60).

The optical band gap of the prepared material was obtained by using Tauc's [**26**] relation shown in **Fig. 7**.

$$(\alpha h\nu)^{1/n} = A(h\nu - E_g) \quad (3)$$

where α denotes absorption coefficient, hν defines the photon energy, E_g is the optical bandgap and A is a constant normally associated with the parameter of edge width reflecting thin film quality. The value of n has different value representing different transition types. The transition from n with a value of ½ and 2 defines the direct allowed transition, while 3 and 3/2 shows indirect allowed transition, indirect forbidden transition and the direct forbidden transition respectively. In present study we have taken n=1/2 that defines the studied compound follows direct allowed transition.

The extinction coefficient is a fundamental optical parameter. It measures the decrease in the emitting light due to absorption coefficient and attenuation and can be calculated using the accompanying formula [**27**]

$$k = \alpha\lambda/4\pi \quad (4)$$

where α states absorption coefficient of thin film and λ provides the data incident wavelength in the thin films. The incident wavelength (λ) vs extinction coefficient (k) shows in **Fig. 8**.

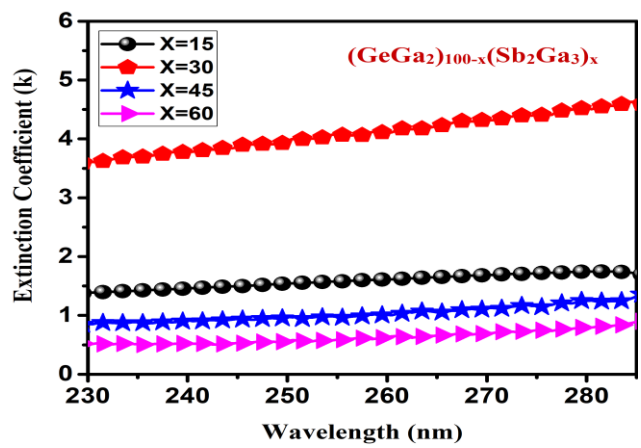

Fig. 8. Variations between coefficient of extinction "k" vs wavelength "λ" of $(Ga_2Ge)_{100-x}$ $(Ga_3Sb_2)_x$ (x = 15,30, 45, 60).

Table 3. Different optical parameters for $(GeGa_2)_{100-x}(Sb_2Ga_3)_x$ (x = 15, 30, 45, 60) thin films.

Composition $(GeGa_2)_{100-x}(Sb_2Ga_3)_x$	Absorption Coefficient α x 10^4 at 2.9 eV	Optical Band gap E_g (eV)	Extinction coefficient k (at 250 nm)	Urbach energy E_u (eV)
x= 15	1.13	2.94 ± 0.13	1.53	0.92
x= 30	2.34	1.97 ± 0.09	3.95	1.32
x= 45	3.94	1.49 ± 0.12	0.95	2.83
x= 60	7.03	1.24 ± 0.08	0.58	3.56

The linear part of the Tauc plot was interpreted at hν→0 for finding the value of optical bandgap of the prepared semiconducting material. The band gap for $(Ga_2Ge)_{100-x}$ $(Ga_3Sb_2)_x$ (x=15, 30, 45, 60) is given in **Table 3**. From **Table 3** it is clear that addition of Sb decreases the bandgap of the material. The decreasing bandgap can be explained using Mott and Davis [**28**] model. According to this model, increasing Sb concentration leads to increase in defect states that defines localized state in the bandgap and hence optical bandgap of the material decreases. The present finding is in good accordance with the findings previously stated by other researchers [**29-32**].

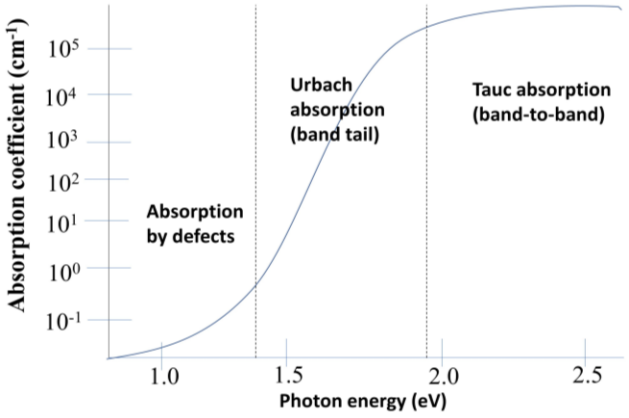

Fig 9. Three different regions of amorphous materials for optical absorption spectra.

There are three distinct regions of amorphous materials for optical spectra of absorption as shown in **Fig. 9**.

- $\alpha \leq 10^2$ cm^{-1}, have region of low energy of absorption. Defects and impurities are present in this area.
- $\alpha \geq 10^4$ cm^{-1} is a region of higher absorption where E_g takes place in between the conduction band and the valance band.
- $\alpha = 10^2$–10^4 cm^{-1}, describing the Urbach exponential tail.

The value of Urbach Energy can be found by following expression.

$$\alpha \sim \exp A(h\nu - h\nu_0)/kT \quad (4)$$

where A is a constant, ν_0 is the lowest frequency of excitation.

The empirical correlation between Urbach's energy [**33,34**], its band tail width from a localized state (Eu) close to the band edges could be determined as

$$A=\alpha_0 \exp(h\nu/Eu) \quad (5)$$

where, α_0 is a constant while E_u stand for Urbach energy [**35**]. **Fig. 10** shows the variation between ln(α) and photon energy (hν) of synthesized thin films. The inverse of slopes of linear region in the graph ln (α) versus photon-energy(hν) graph gives the value of Urbach energy (E_u). Urbach energy (E_u) represents the enhancement of the absorption edge.

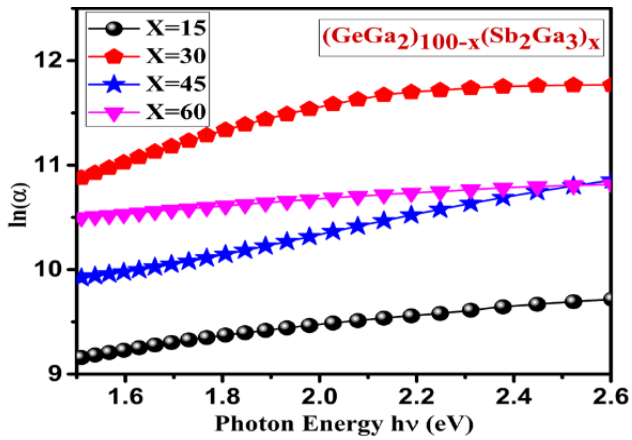

Fig 10. Variation of photon energy vs ln(α) of $(Ga_2Ge)_{100-x}(Ga_3Sb_2)_x$ thin films glassy alloy.

There is decrease in value of optical band gap (E_g) whereas the energy of Urbach (E_u) increases significantly with the high doping concentration of Sb which is shown in **Fig. 11**. The decrease in band gap with the higher doping concentration of Sb may be due to an increase in grain sizes and a decrease in thin film structural impairment. The value of Urbach energy increases which can be attributed to the decrease in structural disorder in the films and also shows reverse behaviour as of energy gap [**36**].

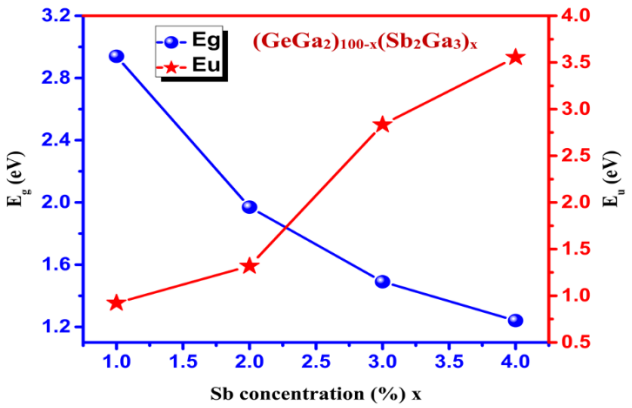

Fig 11. Shows the variation of Sb concentration E_g and E_u for $(Ga_2Ge)_{100-x}(Ga_3Sb_2)_x$ (x = 15,30, 45, 60) E_g and E_u.

Conclusion

High purity $(Ga_2Ge)_{100-x}(Ga_3Sb_2)_x$ (x = 15, 30, 45, 60) 5N (99.999 %) alloy were synthesized using the conventional melt quenching technique. Amorphous bulk glasses $(Ga_2Ge)_{100-x}(Ga_3Sb_2)_x$ (x = 15, 30, 45, 60) were used to thermal evaporation technique for synthesis thin films. The measured value of k, E_g decreases while alpha and Eu increases with increased concentration of doping Sb. Mott and Davis Defect Density Model were used to examine the decrease in the optical band gap with an increase in Sb concentration. The investigated materials could be a good contender for applications in infrared devices. It was noted that the maximum transition in optical constants occurs at x=15. So, $(Ga_2Ge)_{100-x}(Ga_3Sb_2)_x$ is the adaptive composition of IR devices.

Keywords

Non-oxide glass, optical bandgap, FTIR, urbach energy, structural morphology.

Received: 23 March 2021
Revised: 15 May 2021
Accepted: 29 May 2021

References

1. Sharma, I.; Hassanien, A. S.; *Jr. of Non-Cryst, Sol.*, **2020**, *548*, 120326.
2. Hassanien, A.S.; Sharma I.; Aly, K.A.; Physica B: *Condensed Matter*, **2021**, *613*, 412985.
3. Radaf, I. M. El; Al-Zahrani, H. Y. S.; Hassanien, A. S.; *Jr. of Mat. Sci.: Mat. in Elec.* **2020**, *31*, 8336.
4. Singh, P. K.; Shukla, N.; Rao, V.; Dwivedi, D. K.; *Advanced Science, Engineering and Medicine*, **2020**, *12*, 31.
5. Hassanien, A.S.; Radaf, I. M. E.; Akl, A. A, *Jr. of Al. and Com.* **2020**, *849*, 156718.
6. Tintu, R.; Nampoori, V. P. N.; Radhakrishnan, P.; Thomas, S.; *Journal of Applied Physics*, **2010**, *108*, 073525.
7. Karaksina, E.V.; Shiryaev, V.S.; Filatov, A.I., Plekhovich, A.D.; Stepanov, B.S.; Kurganova, A.E.; Nezhdanov, A.V.; Sidorenko, K.V.; *Optical Materials*, **2020**, *104*, 109943.
8. Singh, P. K.; Dwivedi, D. K.; Alharthi, F.A.; Marghany, A.E.; *Nanoscience and Nanotechnology Letters*, **2020**, *12*, 720.
9. Iovu, M.S.; Boolchand, P.; Georgiev, D.G.; *Journal of Optoelectronics and Advanced Materials*, **2005**, *7*, 763.
10. Othman, A.A.; Amer, H.H.; Osman, M.A.; Dahshan, A.; *Radiation Effects & Defects in Solids*, **2004**, *159*, 659.
11. Petit, L.; Carlie, N.; Adamietz, F.; Couzi, M.; Rodriguez, V.; Richardson, K.C.; *Materials Chemistry and Physics*, **2006**, *97*, 64.
12. Dwivedi, P.K.; Tripathi, S.K.; Pradhn, A.; Kulkarni, Agarwal, S.C.; *Journal of Non-Crystalline Solids*, **2000**, *266*, 924.
13. Tverjanovicha, A.S.; Borisov E.N.; Volobueva, O.; Mamedov, S.B.; Mikhailov, M.D.; *Glass Physics and Chemistry*, **2006**, *32*, 677.
14. Tintu, R.; Nampoori, V.P.N.; Radhakrishnan, P.; Thomas S.; *Optics Communications*, **2011**, *284*, 222.
15. Li, Z.B.; Lin, C.G.; Qu, G.S.; Nie, Q.H.; Xu, T.F.; Dai, S.X.; *J. Am. Ceram. Soc.*, **2014**, *97*, 793.
16. Lin, C.G.; Li, Z.B.; Gu, S.X.; Tao, H.Z.; Dai, S.X.; Nie, Q.H.; *J. Wuhan Univ. Technol.*, **2014**, *29*, 9.
17. Wang, S.X.; Davies, R. L.; et al.; *Applied Physics A*, **2013**, *13*, 575.
18. Raj, R.; Lohia, P.; Dwivedi, D. K., *Optik*, **2020**, *218*, 165041.
19. Němec, P.; Olivier, M.; Baudet, E.; Kalendova, E. Benda, P.; Nazabal, V.; *Mater. Res. Bull.*, **2014**, *51*, 176.
20. Vogel, E.M.; Weber, M.J.; Mon Krol, D.; **1991**, *32*, 231.
21. Nathan Carlie, N.C.; Anheier Jr.; Qiao, H. A.; Bernacki, B. et.al.; *Rev. Sci. Instrum*, **2011**, *82*, 053103.
22. Swanepoel, R.; *J. Phys. E*, **1984**, *17*, 896.
23. Imran, M.M.A.; Lafi, O. A.; *Physica B Condens. Matter*, **2013**, *410*, 201.
24. Singh, P. K.; Tripathi, S.K.; Dwivedi, D.K.; *Mater. Sci.*, **2019**, *37*, 554.
25. Tauc, J.; Amorphous and Liquid Semiconductors, Plenum, New York, 1**974**, p.171.
26. Hassanien, A.S.; Sharma, I.; *Optik*, **2020**, *200*, 163415.
27. Mott, N.F.; Davis, E.A.; Electronics Processes in Non – Crys Mat, Clarendon, Oxford, **1979**, p. 428.
28. Li, Z.B.; Lin, C.G.; G.S. Qu, Q.H. Nie, T.F. Xu, S.X. Dai, *J. Am. Ceram. Soc.*, **2014**, *97*, 793.
29. Lin, C.G.; Li, Z.B.; Gu, S.X.; Tao, H.Z.; Dai, S.X.; Nie, Q.H.; *J. Wuhan Univ. Technol.*, **2014**, *29*, 9.
30. Carlie, N.; Musgraves, J.D.; Zdyrko, B.; Luzinov, I.; Hu, J.J.; Singh, V.; Agarwal, A.; Kimerling, L.C.; Canciamilla, A.; Morichetti, F. Melloni, A.; Richardson, K.; *Opt. Express*, **2010**, *18*, 26728.
31. Petit, L.; Carlie, N.; Adamietz, F.; Couzi, M.; Rodriguez, V.; Richardson, K.C.; *Mater. Chem. Phys.*, **2006**, *97*, 64.
32. Musgraves, J.D.; Carlie, N.; Hu, J.'; Petit, L.; Agarwal, A.; Kimerling, L.C. Richardson, K.A.; *Acta Mater.*, **2011**, *59*, 5032.
33. Huang, C.C. Wu, C.C.; Knight, K.; Hewak, D.W.; *J. Non-Cryst. Solids*, **2010**, *356*, 281.
34. Song, S.S.; Carlie, N.; Boudies, J.; Petit, L.; Richardson, K.; Arnold, C.B.; *J. Non-Cryst. Solids*, **2009**, *355*, 2272.
35. Novak, J.; Novak, S.; Dussauze, M.; Fargin, E.; Adamietz, F.; Musgraves, J.D.; Richardson, K.; Mater. Res. Bull. **2013**, *48*, 1250.
36. Knotek, P.; Navesnik, J.; Cernohorsky, T.; Kincl, M.; Vlcek, M.; Tichy, L.; *Mater. Res. Bull.*, **2015**, *64*, 42.